

Encapsulated Corrosion Inhibitive Pigment for Smart Epoxy Coating Development: An Investigation of Leaching Behavior of Inhibitive Ions

Zoi Lamprakou, Huichao Bi,* Claus Erik Weinell, and Kim Dam-Johansen



Cite This: *ACS Omega* 2023, 8, 14420–14429



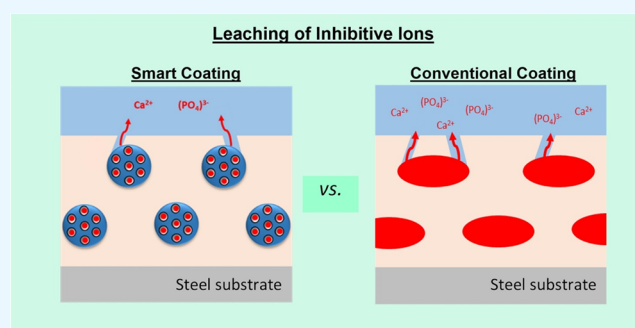
Read Online

ACCESS |

Metrics & More

Article Recommendations

ABSTRACT: A comparative study between the leaching behavior of inhibitive ions from conventionally pigmented and smart (with encapsulated pigments) epoxy coatings has been conducted. Leaching of calcium phosphate as an inhibitive pigment from epoxy coatings was tested in 3.5 wt % NaCl solution. The results showed that pigment encapsulation contributed to a more uniform and stable coating microstructure based on the Scanning Electron Microscopy–Energy-Dispersive X-ray Spectroscopy (SEM-EDX) analysis and a higher leaching rate of the inhibitive pigment via the Inductively Coupled Plasma Optical Emission Spectroscopy (ICP-OES) analysis, thereby enhancing both the active corrosion protection and the barrier properties of the coating film. This was further verified by the Electrochemical Impedance Spectroscopy (EIS) measurements. After 7 days of immersion in 3.5 wt % NaCl solution, the coating resistance of the smart epoxy coating with mesoporous silica nanoparticle encapsulated calcium phosphate (MSN-CP3%) was $2 \times 10^9 \Omega \cdot \text{cm}^2$ compared to $1.1 \times 10^6 \Omega \cdot \text{cm}^2$ and $2.6 \times 10^6 \Omega \cdot \text{cm}^2$ for the conventional epoxy coatings pigmented with 3 wt % and 5 wt % calcium phosphate (CP3% and CP5%), respectively.



1. INTRODUCTION

Organic coatings protect metal structures from corrosion by acting as a physical barrier between the substrate and the aggressive environment. The organic resin together with barrier pigments restricts the transportation of corrosive ions to the substrate and increases the ionic resistance between the local anodes and cathodes on the surface of the substrate.^{1,2} However, coating films are rarely defect-free.³ In addition, exposure time and interactions with the environment can either exacerbate the initial defects or generate new ones, compromising the barrier properties of the coating.⁴

One way to improve coatings' anticorrosive performance is to incorporate inhibitive pigments into coating formulations.^{5,6} Active inhibitive pigments are sparingly soluble in water. When water penetrates the coating film, it dissolves part of the inhibitive pigments, and the inhibitive ions can travel to the coating/metal interface and obstruct corrosion by forming a protective layer with the metal substrate.^{7,8} To achieve a sufficient inhibition action, a fast and adequate supply of inhibitive ions is needed during the early exposure stages to form the inhibitive film. Later, a lower concentration may be required to maintain the inhibitive film.⁹ However, in a conventional coating with inhibitive pigments, extended exposure to wet conditions can influence the release and transport of the inhibitive species which may lead to a fast depletion of the

coating from the inhibitive pigment, thereby sacrificing the barrier properties of the coating film.¹⁰ Therefore, to ensure sufficient long-term inhibitive protection, a higher pigment concentration is needed.¹¹ Another solution to ensure sufficient inhibitive species and to minimize undesired losses is the controlled release of the inhibitive species from a smart carrier.¹² Smart carriers such as polymeric capsules,¹³ halloysites,¹⁴ or mesoporous nanoparticles^{15,16} work as reservoirs for the inhibitive species.^{17,18} When corrosion reactions take place, the local increase in the pH can trigger the release.^{19,20} Coatings that are capable of adapting their properties according to environmental changes such as in pH, temperature, pressure, surface tension, mechanical forces, etc. are called smart coatings.²¹ The controlled pigment release can prolong the coating's durability by eliminating the spontaneous leaching of the inhibitive species from the coating film and by enhancing their barrier properties.²²

Received: December 9, 2022

Accepted: March 30, 2023

Published: April 11, 2023



Zinc chromate, ZnCrO_4 , and red lead, Pb_3O_4 , were historically two of the most effective inhibitive pigments. However, their toxicity and resulting environmental contamination led to their replacement.^{23,24} Several alternatives have been tested, among which zinc phosphate, $\text{Zn}_3(\text{PO}_4)_2$, is the most widely applied inhibitive pigment in coatings formulation. Also, phosphate compounds with Zn^{2+} coupled with secondary cations have also been applied for the development of coatings to enhance their corrosion inhibition.^{25–28} Nevertheless, alternatives in the absence of zinc are preferred due to the adverse effects that may be caused by the zinc compounds to the aquatic life. Researchers are actively seeking substitutions to zinc complexes, such as Al,^{29,30} Sr,³¹ Ca,^{32–34} and ammonium³⁵ complexes for corrosion inhibition.

Direct addition of corrosion inhibitors into the coatings can result in uncontrollable consumption, i.e. too low concentration of the pigment to initiate corrosion inhibition due to low solubility or fast depletion of inhibition efficiency and coating integrity damage due to high solubility of the pigment. Controlled release techniques therefore have drawn more and more attention.^{14,15,36–38} Encapsulation of the corrosion inhibitors with (nano)containers is one effective controlled release strategy. Although there has been a growing interest in the incorporation of encapsulated corrosion inhibitors into coatings' development, investigations on the leaching behavior of inhibitive pigments from organic coatings and the effect of the encapsulation are limited. Learning how the inhibitive pigments leach from the coating can help to better design the coating formulation with controlled release technology toward more efficient and longer-lasting corrosion protection. Prosek et al.³⁹ investigated the leaching kinetics of chromate inhibitive pigments from polyester-isocyanate coatings. The leaching rate of chromate ions from the coating into water solutions showed a logarithmic dependence of chromate ion concentration connected to the diffusion of the solution through the coating. However, their study showed that the rate-determining step of the leaching was probably the initial dissolution of the chromate from the inhibitive pigment particles. Furman et al.⁹ analyzed the leaching profiles of chromate-pigmented epoxy-polyamide coatings. Four methods were employed to fit the leaching data: Fick's second law of diffusion, the power law, a third-order polynomial equation, and the shrinking core model. Non-Fickian diffusion kinetics were observed with the polynomial model, and power law models exhibited the best fit of chromate ion concentration dependency. The fitting of the power law showed that there was a first-order reaction taking place in the system which slowed down the diffusion at longer times. Additionally, the leaching of strontium aluminum polyphosphate hydrate (SAPH) from polyester–polyisocyanate coatings was investigated by Emad et al.^{2,40,41} In these studies, an increased pigment concentration was connected to a higher leaching concentration of inhibitive ions. However, the accumulation of electrolyte at the pigment/binder interface influencing the coating microstructure was proposed to be the main factor related to pigment leaching. The higher leaching concentration was also connected to lower impedance values of the coatings due to the formation of voids in the coating film. The voids were filled up with the electrolyte, thereby generating conductive paths for the aggressive species (such as water and oxygen) to travel to the metal substrate.

The overall aim of this work is to better understand the influence of pigment encapsulation on the leaching of the inhibitive species from the coating film. In a recent work,³⁸ we

identified that pigment encapsulation can increase the barrier properties of an epoxy coating compared to conventionally pigmented coatings. Calcium phosphate, $\text{Ca}_3(\text{PO}_4)_2$ was used as a commercially available inhibitive pigment and was encapsulated into mesoporous silica nanoparticles (MSN). The pH-triggered response of calcium phosphate-loaded MSN particles (MSN-CP) was proven. Conventional coatings pigmented with calcium phosphate and smart coatings with loaded MSN particles were exposed to the salt spray chamber and evaluated by Electrochemical Impedance Spectroscopy (EIS). The smart coating showed better anticorrosive performance than the conventionally pigmented coatings. In this study, further research has been undertaken to identify the influence of inhibitive pigment encapsulation into MSN on the leaching profile of the inhibitive ions from the coating film. The difference in the leaching rate has an influence on both the barrier properties of the coating by altering the coating microstructure and the active corrosion protection by ensuring sufficient inhibitive ion concentration. Leaching rates and EIS measurements have been conducted and compared on the epoxy coatings with nonencapsulated and encapsulated inhibitive pigments after immersion in a 3.5 wt % NaCl solution.

2. EXPERIMENTAL SECTION

2.1. Coating Formulation and Coated Panel Preparation. Two types of coatings were formulated for this study, one group referring to conventionally pigmented coatings and one group to coatings with encapsulated inhibitive pigment. Calcium phosphate (Heubach, GmbH) was used as an inhibitive pigment in both groups. The main characteristic properties of the calcium phosphate used are listed in Table 1.⁴²

Table 1. Main Characteristic Properties of the Commercial Calcium Phosphate Pigment from Heubach GmbH. Reproduced with Permission from Reference 42

Density (g/cm^3)	2.9
Average particle size (μm)	2.5–4
Oil absorption value ($\text{g}/100 \text{ g}$)	40

The procedure followed for the synthesis and the loading of the MSN particles with calcium phosphate was the same as presented in our previous study.³⁸ A standard sol–gel method was used for the synthesis of the MSN particles, with hexadecyltrimethylammonium bromide (CTAB) employed as the surfactant and tetraethyl orthosilicate (TEOS) as the precursor in the process. After the synthesis, the MSN particles were calcined in air at 550 °C for 6 h. The loading of calcium phosphate into the MSN particles took place in acidic conditions (pH 2) from a saturated calcium phosphate solution.

The solution was stirred for 24 h, then filtered with glass microfibers filters with a pore size of 1.2 μm (Grade GF/D, Sigma-Aldrich) to remove calcium phosphate residues. The MSN particles were added to the solution and stirred for 28 h. The suspension was then filtered in a vacuum assembly, and the filtration product was left to dry in the oven at 45 °C overnight. The average particle size was measured by SEM images to be 447 and 550 nm before and after loading, respectively.

The epoxy coating formulations in each case are given in Table 2,³⁸ where the epoxy resin used is a high solid bisphenol A epoxy binder and the curing agent a 10% adducted polyamide. The formulated coating was applied on smooth mat mild steel panels (Q panels from TQC sheen, 75 × 150 × 0.8 mm) using a

Table 2. Coatings Base and Curing Composition. Reproduced with Permission from Reference 38

	Coating	Abbreviation	Components	Mass (%)
Base formulations	Calcium phosphate 3 wt % epoxy coating	CP3%	Epoxy resin	55.7
			Plasticizer	22.1
			Wetting agent	1.5
			Solvents	17.1
			Calcium phosphate	3.6
	Calcium phosphate 5 wt % epoxy coating	CP5%	Epoxy resin	54.0
			Plasticizer	22.5
			Wetting agent	1.5
			Solvents	16.6
			Calcium phosphate	6.4
MSN loaded with calcium phosphate 3 wt % epoxy coating	MSN-CP3%	Epoxy resin	55.7	
		Plasticizer	22.1	
		Wetting agent	1.5	
		Solvents	17.1	
		MSN-CP	3.6	
Adducted curing agent ^a			3-(diethylamino) propylamine	63.6
			Epoxy resin	12.9
			Solvent	23.5

^aThe mixing ratio of the base and the curing is 5:1 by volume for all the formulations.

draw-down film applicator. The dry film thickness (DFT) was $80 \pm 5 \mu\text{m}$ for all the samples (Elcometer 355 Precision Coating Thickness Gauge, Elcometer Inc.). The panels were left to fully cure for 2 weeks in a ventilation chamber at $20 \pm 2 \text{ }^\circ\text{C}$.

A cutting setup (Secotom-6, Struers A/S) was used to cut the cured coated panels into the size of 4 cm \times 4 cm. The backside and the edges of the panels were sealed by using a commercial epoxy coating for heavy-duty service with a high solid polyamide epoxy coating and an extra waterproof masking tape as needed. A minimum of 2 panels were prepared for all the tests in this work as reproducibility checks.

2.2. Coatings Exposure and Inhibitive Pigment Leaching Measurements. Coated panels were immersed in 3.5 wt % NaCl solution at $20 \pm 2 \text{ }^\circ\text{C}$ for 7 days. The 3.5 wt % NaCl solution was prepared with analytical reagent grade >99.0% sodium chloride (Merck KG) and deionized water. The coated samples were placed horizontally at the base of a 250 mL plastic container filled with 200 mL of electrolyte. Small (2 mL) leaching aliquots were removed after 0, 6 h, and 1, 2, 3, 5, and 7 days of immersion, and the cumulative concentration of Ca^{2+} in the solutions was determined by inductively coupled plasma optical emission spectroscopy, ICP-OES (iCAP 7200, Thermo Scientific).

2.3. Evaluation of the Anticorrosive Performance of the Coatings. The corrosion-resistant performance was evaluated by EIS measurements, with a three-electrode cell setup (the coated steel panel as the working electrode, a saturated calomel electrode (SCE) as the reference electrode, and a graphite rod as the counter electrode) by Reference 600+ potentiostat (Gamry Instruments, USA). EIS measurements were conducted, with respect to the open circuit potential, with an amplitude of sinusoidal voltage of 10 mV and a frequency range of 100 kHz to 0.1 Hz in 3.5 wt % NaCl solution at $20 \pm 2 \text{ }^\circ\text{C}$ and a 10 cm^2 tested area. The EIS data were analyzed by Gamry Echem Analyst software.

2.4. Characterization of the Microstructure of the Coatings. Microstructural changes and elemental composition of the unexposed and exposed coatings were characterized from the top surface of the samples. Scanning electron microscopy (SEM) and the Energy-dispersive X-ray spectroscopy (EDS) analyses were performed in high vacuum mode by Prisma E SEM from ThermoFisher Scientific. Before the SEM and the EDS analysis, samples were sputtered with silver.

3. RESULTS AND DISCUSSION

3.1. Electrochemical Evaluation of the Coating Performance. Figure 1 shows the Bode plots of the CP3%, CP5%, and MSN-CP3% coatings that were immersed for 7 days in 3.5 wt % NaCl solution. The MSN-CP3% coating presents one time constant, which shows high capacitive behavior throughout the immersion time, indicating good barrier properties.⁴³ The CP3% and CP5% coatings exhibited a significant decrease in the coating impedance over the immersion time, and a second time constant element appeared after day 1, indicating the initiation of corrosion reactions at the coating/metal interface.

To further understand and explain the differences and the mechanisms of the anticorrosive performance of the coatings, two equivalent circuit models, $R(\text{QR})$ and $R(\text{Q}(\text{R}(\text{QR})))$, were applied to fit the data depending on the different processes involved, as shown in Figure 2. In the models, R_s is the solution resistance; R_f is the film resistance; R_{ct} is the charge transfer resistance; Q_f is the constant phase element corresponding to film capacitance (Y_f and n_f are the associated parameters of Q_f); and Q_{dl} is the constant phase element corresponding to double-layer capacitance (Y_{dl} and n_{dl} are the associated parameters of Q_{dl}). Table 3 shows the fitted data of R_f , Y_f , n_f , R_{ct} , Y_{dl} , and n_{dl} by Gamry Echem Analyst.

The film resistances for different coatings over the immersion period are shown in Figure 3a. It is clearly shown that the coating with MSN-CP3% has a higher film resistance over the immersion time, i.e. $10^{10} \Omega \cdot \text{cm}^2$ for the first 2 days and $10^9 \Omega \cdot \text{cm}^2$ even after 7 days of immersion, thus providing better barrier protection. The small decrease observed from day 2 to day 3 can be correlated to the creation of new electrolyte-filled pores (voids) in the coating matrix due to water diffusion along the heterogeneities of the coating film. For the conventional coatings, CP3% and CP5%, the R_f drops significantly during the first 2 days of exposure (from $10^{10} \Omega \cdot \text{cm}^2$ at day 0 to $10^7 \Omega \cdot \text{cm}^2$ at day 2), showing the reduced barrier protection of those coatings.⁴⁴ The decrease in the barrier properties of the coating films in the case of the conventional coatings can be related to the partial dissolution of the pigment and the accumulation of water in the forming voids.

The film capacitance gives an indication of the water uptake into the coating. Water permeation can result in swelling of the coating and the initiation of blisters or delamination.⁴⁵ The film capacitances for the three coatings with respect to the immersion period are shown in Figure 3b. For all the coatings, the capacitive parameter, Y_f which is associated with the coating film capacitance, Q_f remains almost stable during the immersion period at $10^{-9} \sim 10^{-10} \text{ F} \cdot \text{s}^{-1} \cdot \text{cm}^{-2}$ with close n values, suggesting the water had largely saturated the coatings within a short period of time upon immersion in the electrolyte.

The fitting values of the R_{ct} and the Y_{dl} from the circuit model $R(\text{Q}(\text{R}(\text{QR})))$ are also listed in Table 3. The presence of the second time constant shows that corrosion reactions take place. The Y_{dl} values indicate there is greater surface coverage of the

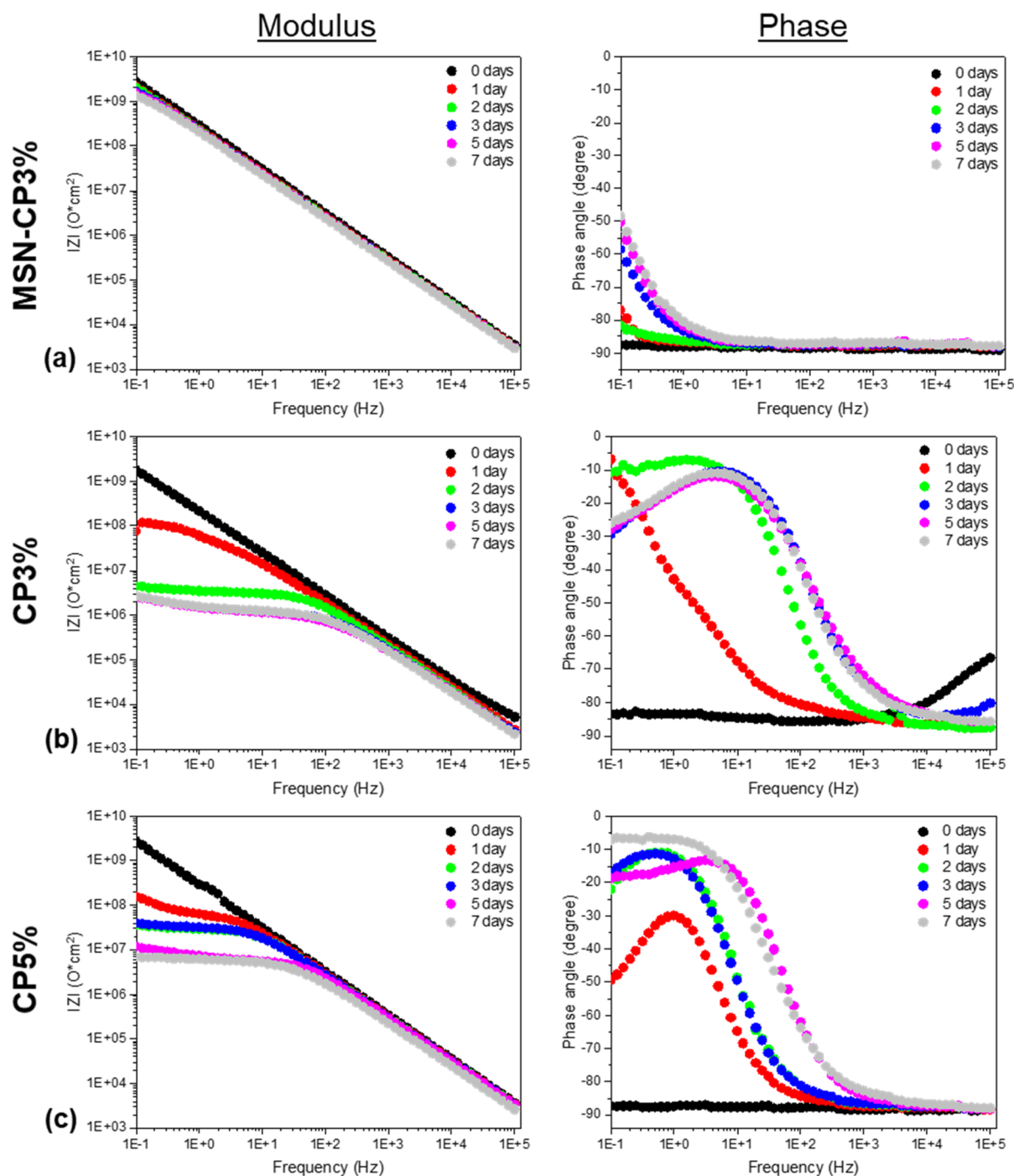


Figure 1. Bode plots of (a) MSN-CP3%, (b) CP3%, and (c) CP5% coatings as a function of immersion time in 3.5 wt % NaCl solution.

mild steel substrate by the formed inhibiting layer in the case of coating with CP5% compared to coating with CP3%, as the Y_{dl} for CP5% is 1 order of magnitude lower than that for CP3% after 7 days of immersion. The increased surface coverage in the case of CP5% is probably due to the higher pigment concentration in the coating that can ensure sufficient inhibitive ions for mild steel corrosion protection.

3.2. Leaching Measurements of the Inhibitive Ions from Epoxy Coatings. Leaching measurements of the inhibitive ions from epoxy coatings were performed for each of the three formulated coatings. The cumulative release profile of calcium ions from the CP3% and CP5% coatings are presented in Figure 4. The time dependence of the calcium

concentration shows a logarithmic correlation for both coatings. Thus, Fick's second law of diffusion is applied to express the release rate of calcium ions. According to Prosek et al.,³⁹ based on the inhibitive ions, the concentration of the released inhibitive pigment from the exposed coating can be expressed as

$$C_{Ca} = k \ln(t) + a \quad (1)$$

Where k shows the release rate, and a is a constant with no simple physical meaning but is likely connected to the fast dissolution of the inhibitive pigment close to the coating surface due to the concentration gradient between the coating and the environment (aqueous solution). In Figure 4, the dashed lines show the linear fit of each sample. The parameters k and a

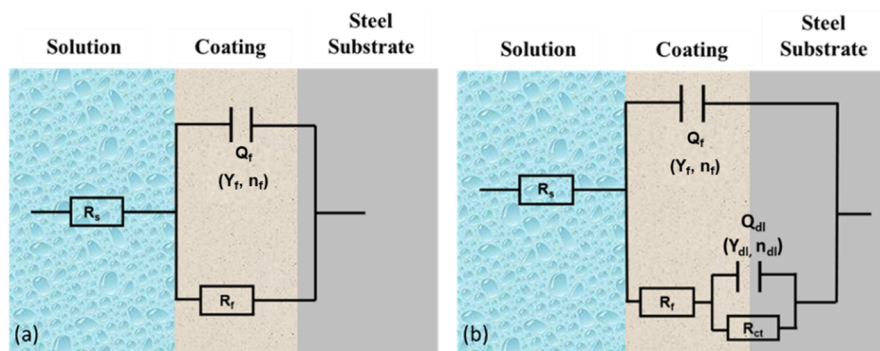


Figure 2. Equivalent circuit models applied to the data, (a) R(QR) and (b) R(Q(R(QR))).

Table 3. EIS Fitting Data with the Equivalent Circuit Models

Sample	Days	Fitted model	Impedance parameters					
			R_f ($\Omega \cdot \text{cm}^2$)	Y_f ($\text{F} \cdot \text{s}^{n_f-1} \cdot \text{cm}^{-2}$)	n_f	R_{ct} ($\Omega \cdot \text{cm}^2$)	Y_{dl} ($\text{F} \cdot \text{s}^{n_{dl}-1} \cdot \text{cm}^{-2}$)	n_{dl}
MSN-CP3%	0	R(QR)	9.5×10^{10}	5.6×10^{-10}	0.98			
	1	R(QR)	1.3×10^{10}	7.1×10^{-10}	0.97			
	2	R(QR)	1.7×10^{10}	7.5×10^{-10}	0.97			
	3	R(QR)	3.3×10^9	7.6×10^{-10}	0.97			
	5	R(QR)	2.2×10^9	7.9×10^{-10}	0.97			
CP3%	7	R(QR)	2×10^9	8×10^{-10}	0.96			
	0	R(QR)	4×10^{10}	8.2×10^{-10}	0.94			
	1	R(Q(R(QR)))	4×10^7	1.2×10^{-9}	0.94	6.8×10^7	2.4×10^{-9}	0.82
	2	R(Q(R(QR)))	2.9×10^6	1.1×10^{-9}	0.96	1.9×10^7	6.6×10^{-7}	0.35
	3	R(Q(R(QR)))	1.1×10^6	1.7×10^{-9}	0.92	4.6×10^{11}	7×10^{-7}	0.50
CP5%	5	R(Q(R(QR)))	1×10^6	2×10^{-9}	0.91	5.3×10^{11}	6.7×10^{-7}	0.41
	7	R(Q(R(QR)))	1.1×10^6	1.8×10^{-9}	0.92	2.2×10^{11}	7×10^{-7}	0.46
	0	R(QR)	8.5×10^{10}	5.5×10^{-10}	0.96			
	1	R(Q(R(QR)))	6.2×10^7	6.5×10^{-10}	0.97	1×10^9	1×10^{-8}	0.81
	2	R(Q(R(QR)))	2.9×10^7	7×10^{-10}	0.96	4.3×10^{12}	9.9×10^{-8}	0.72
	3	R(Q(R(QR)))	3.1×10^7	7.1×10^{-10}	0.97	7.8×10^{12}	8.8×10^{-8}	0.58
	5	R(Q(R(QR)))	5.4×10^6	7.1×10^{-10}	0.96	1.5×10^7	1.2×10^{-7}	0.54
7	R(Q(R(QR)))	2.6×10^6	1×10^{-9}	0.96	4.4×10^7	8.1×10^{-8}	0.55	

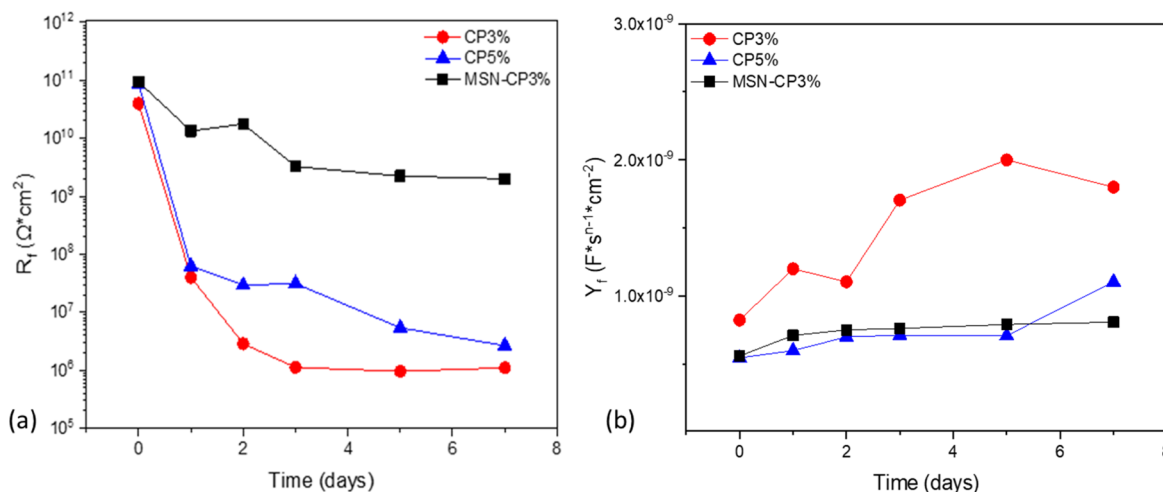


Figure 3. (a) The film resistance (R_f) and (b) the film capacitance (Y_f) of the CP3%, CP5%, and MSN-CP3% coatings over the immersion time in 3.5 wt % NaCl solution.

together with the coefficient of determination, R^2 , of the fitted equation are listed in Table 4.

The comparison between the CP3% and CP5% coatings showed that the increased inhibitive pigment concentration led to a faster release rate during exposure (immersion in 3.5 wt %

NaCl solution), i.e., a k value of 0.13 mg/L for the CP5% and 0.08 mg/L for the CP3% samples. The ratio of the release rates ($0.13/0.08 = 1.62$) is close to the ratio of the pigment concentration ($5 \text{ wt } \%/3 \text{ wt } \% = 1.66$), which verifies the correlation between the leaching rate and the pigment

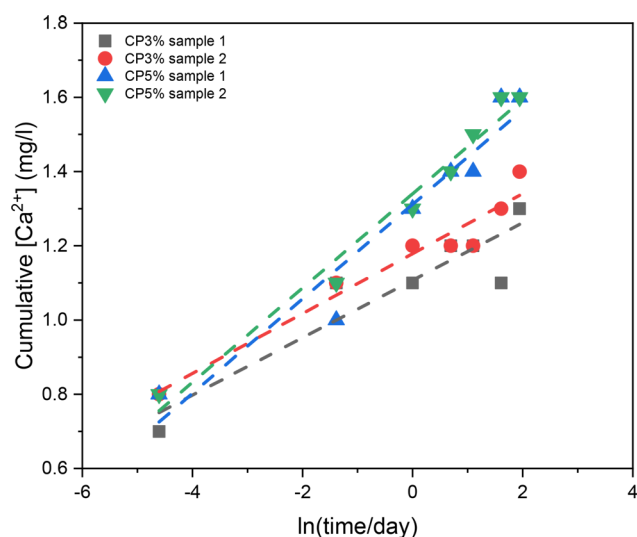


Figure 4. Cumulative concentration of calcium ions leached from the CP3% and CP5% epoxy coatings during 7 days of immersion in 3.5 wt % NaCl solution. Sample 1 and sample 2 are presented as a reproducibility check.

concentration in the coating. Moreover, after 7 days' immersion, the final concentration that calcium ions reached in the solution is higher in the case of CP5% than the CP3% coating. The faster leaching rate and the higher final inhibitive ion concentration in the case of the CP5% coating compared to CP3% can also explain the Y_{dl} values from the EIS data; i.e., the higher availability of inhibitive ions for the CP5% coating led to a higher surface coverage of the steel substrate with the formed protective layer.

The release profile of calcium ions from the MSN-CP3% coatings is shown in Figure 5. The release data showed a transition of the release rate from day 0 to day 2 (Phase I) and from day 2 to day 7 (Phase II). Linear fit of the equation was performed for the two phases separately. According to the fitted values from Table 4, the release constant is 5 times lower during Phase I than Phase II. During Phase I, the k and a values of MSN-CP3% are quite close to those of CP3%. Our previous work indicated that part of the calcium phosphate was adsorbed on the surface of MSN particles.³⁸ Thus, the leaching behavior in Phase I as observed here can be attributed to the dissolution of the adsorbed part of calcium phosphate from the surface of the MSN particles.

That change in the release profile and the increased release rate after day 2 during Phase II can be correlated to EIS results and the controlled release of the inhibitive pigment from the capsules. As the electrolyte travels through the pores and reaches the coating/metal interface, it activates the resistance of the

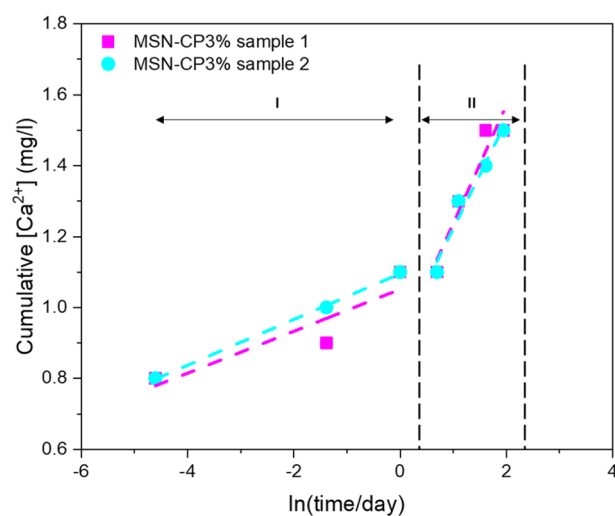


Figure 5. Time dependency of the released calcium from the MSN-CP3% epoxy coatings immersed in 3.5 wt % NaCl solution. Sample 1 and sample 2 are presented as a reproducibility check.

pores leading to the slight bending of the Bode plot (magnitude in the lower frequency range).⁴⁶ The decrease in the R_f value after day 2 for MSN-CP3% as mentioned above can be correlated to the increased coating porosity. Thus, a higher amount of water reaches the coating/metal interface, more cathodic and anodic sites appear, and a higher concentration supply of the inhibitive pigment is needed to effectively suppress the corrosion reactions. The local pH increases due to the presence of cathodic reactions and triggers the release of the inhibitive ions from the MSN-CP nanoparticles, as proved in our previous study (pH-triggering release).³³ Hence, a transition in the release rate of the inhibitive ions from the coating is observed, and the processes taking place in the MSN-CP3% coating during Phase I and Phase II can be schematically represented in Figure 6. The faster release rate due to triggered release can provide the necessary amount of inhibitive ions to effectively suppress the corrosion reaction rates. The protection mechanism is described in reference 38. EIS results also verified this enhanced anticorrosive performance of the MSN-CP3% coating.

3.3. Microstructural Characterization of the Coatings.

Figure 7 shows the top surface of the coated steel panels before and after 7 days of immersion in 3.5 wt % NaCl solution. Before the immersion, MSN-CP3% has the most smooth coating surface without cracks and discontinuities. The SEM images of conventional CP3% and CP5% coatings revealed discontinuities (blue arrows), especially for CP3%, on the top surface of the coating due to the presence of the calcium phosphate pigment. The pigment particles may not be breaking through the coating

Table 4. Fick's Second Law Fitted Parameters Based on Data Presented in Figure 4 and Figure 5^a

Sample name	k (mg/L)		a (mg/L)		R^2	
CP3% sample 1	0.08		1.1		0.94	
CP3% sample 2	0.07		1.1		0.84	
CP5% sample 1	0.13		1.3		0.97	
CP5% sample 2	0.13		1.3		0.93	
MSN-CP3% sample 1	0.06 ^b	0.3 ^c	1.1 ^b	0.9 ^c	0.99 ^b	0.96 ^c
MSN-CP3% sample 2	0.06 ^b	0.3 ^c	1 ^b	0.9 ^c	0.84 ^b	0.92 ^c

^aSample 1 and sample 2 are presented as a reproducibility check. ^bValues refer to the first release phase (Phase I) of the MSN-CP3% coatings.

^cValues refer to the second release phase (Phase II) of the MSN-CP3% coatings.

Pigment leaching processes in the coating film

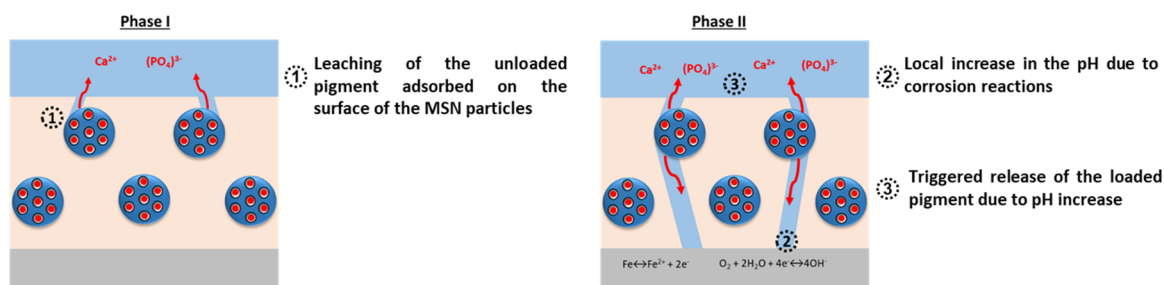


Figure 6. Schematic representation of the pigment leaching processes taking place in the MSN-CP3% coating during Phase I and Phase II.

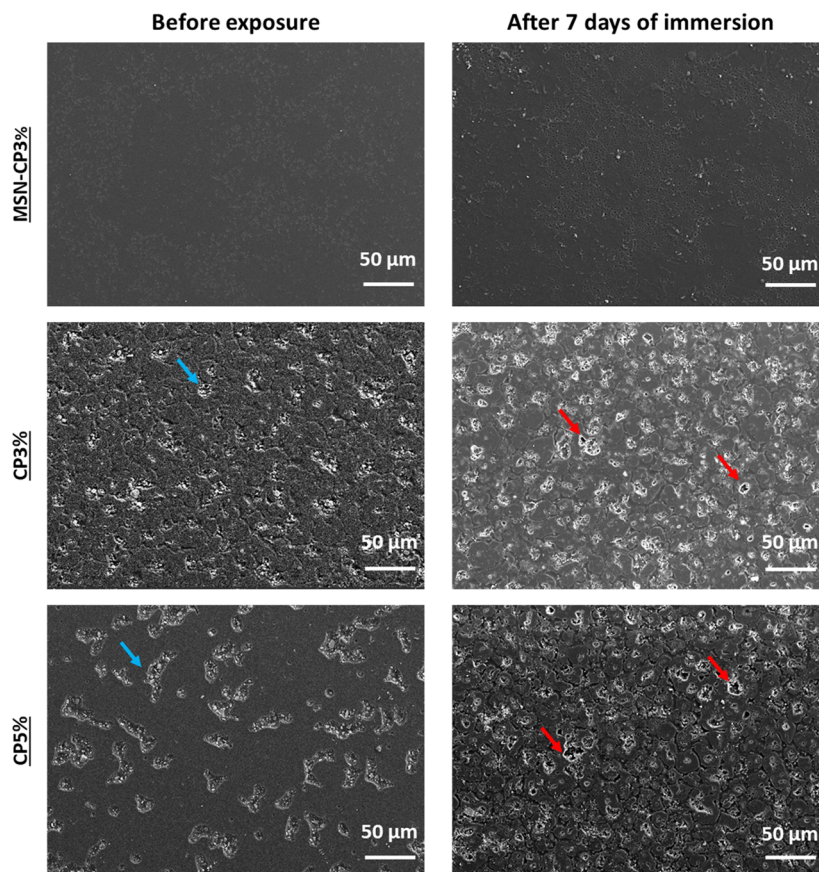


Figure 7. SEM images of the top surface of smart MSN-CP3% and conventional CP3% and CP5% coatings before and after exposure. The blue arrows indicate discontinuities before exposure due to the presence of the pigment. Red arrows show cavities that formed after immersion in 3.5 wt % NaCl solution for 7 days.

film in the case of CP3% and CP5% coatings but are visible since they are very close to the top surface. The concentration of calcium phosphate being higher near the top surface of the coating in CP5% than in CP3% can be related to the fitted constant a as listed in Table 4 (1.1 mg/L for the CP3% and 1.3 mg/L for the CP5%). The discontinuities of the conventional coatings, especially for CP3%, could be one factor affecting the leaching of the inhibitive pigment. A smoother surface in the case of MSN-CP3% indicates a lower number of defects, leading to lower leaching rates from the top surface of the coatings during the initial immersion time. This conclusion can also be supported by the k values from Table 4. The k value of MSN-CP3% during the first phase is 0.06 mg/L, which is the lowest of

the three coatings, compared to 0.08 mg/L for CP3%, and 0.13 mg/L for CP5%.

The post-exposure SEM images verify that MSN-CP3% did not experience any drastic change in the appearance of the top surface. On the other hand, exposure time had different effects on the CP3% and CP5% coatings. The CP5% coating film appeared to have more cracks and some cavities (red arrows) on the top surface after exposure. This change in appearance can be attributed to pigment dissolution and the formation of paths and voids in the coating film as also implied by the drastic drop in the film resistance (R_f values in Figure 3a). The CP3% coating also experienced some bigger cracks and voids (red arrows) after exposure. However, in the CP3% coating, the presence of light-colored areas around the visual defects indicates the presence of

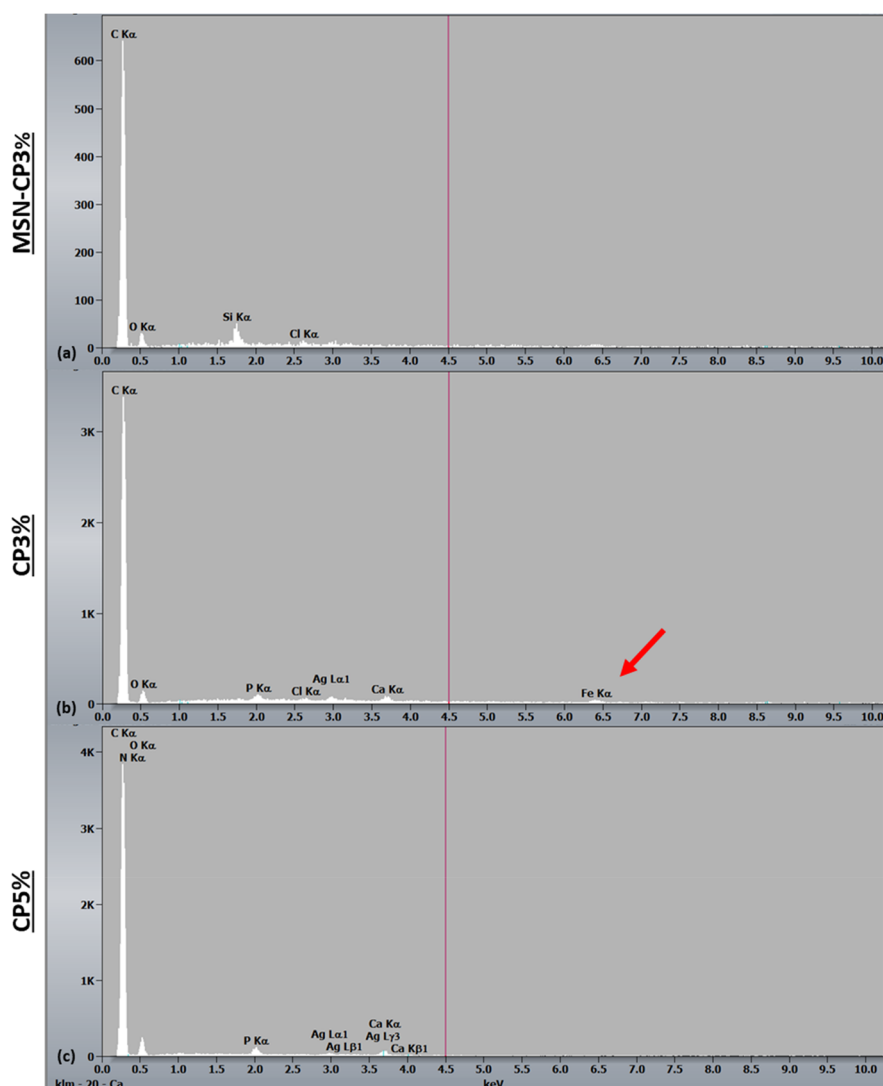


Figure 8. EDS spectra on the top surface of exposed (a) MSN-CP3%, (b) CP3%, and (c) CP5% coatings after immersion in 3.5 wt % NaCl solution for 7 days.

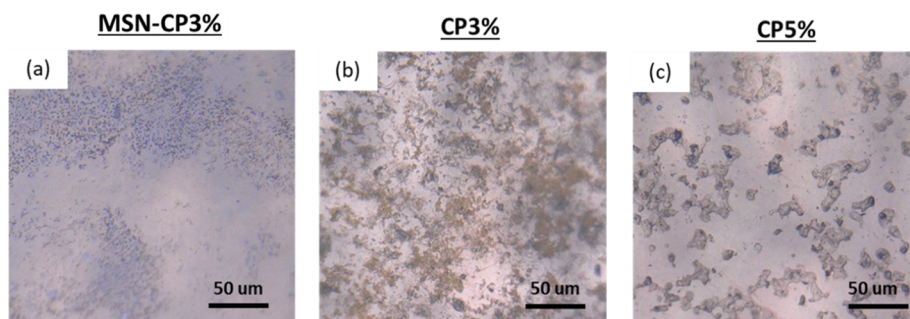


Figure 9. Optical images of (a) MSN-CP3%, (b) CP3%, and (c) CP5% coatings after 7 days of immersion in 3.5 wt % NaCl.

corrosion products. EDS spectra for the three coatings after exposure are presented in Figure 8. The presence of an Fe peak in the EDS spectrum of CP3% proved that corrosion products traveled through the coating to the top surface. Moreover, the optical images (Figure 9) verified the presence of corrosion products on the top surface of the CP3% coating (Figure 9b) after 7 days of immersion in 3.5 wt % NaCl solution.

From the above microstructural characterization (SEM-EDX analysis together with the optical images), it can be concluded

that pigment encapsulation contributes to a more uniform and stable microstructure of the coating before and after exposure to salt solution, and the anticorrosive properties of the coating have been enhanced. This agrees with the EIS measurement results. Direct addition of the nonencapsulated inhibitive pigment led to increased coating porosity due to the dissolution of the pigment particles after exposure.

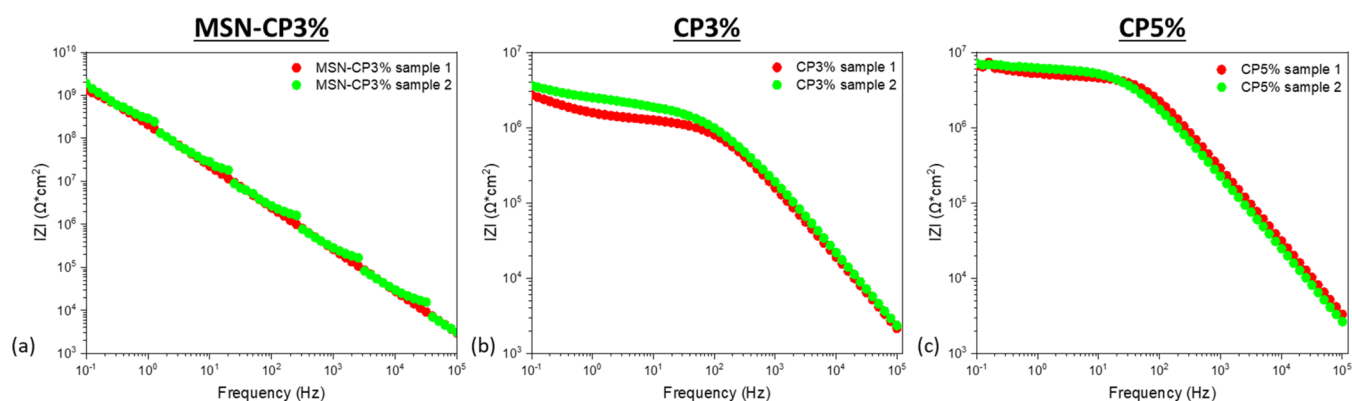


Figure 10. Reproducibility checks. Bode modulus plots of two samples for each formulation (a) MSN-CP3%, (b) CP3%, and (c) CP5% after 7 days of immersion in 3.5 wt % NaCl solution.

4. CONCLUSIONS

The following conclusions can be drawn from this work:

- An epoxy coating with encapsulated calcium phosphate as an inhibitive pigment showed enhanced anticorrosive performance compared to the conventionally pigmented epoxy coatings with the direct addition of calcium phosphate after 7 days of immersion in 3.5 wt % NaCl solution. The coating resistance of MSN-CP3% was $2 \times 10^9 \Omega \cdot \text{cm}^2$ by the end of the experiment, compared to $1.1 \times 10^6 \Omega \cdot \text{cm}^2$ and $2.6 \times 10^6 \Omega \cdot \text{cm}^2$ for CP3% and CP5%, respectively. Additionally, film capacitance was $8 \times 10^{-10} \text{ F} \cdot \text{s}^{-1} \cdot \text{cm}^{-2}$ for MSN-CP3%, $1.8 \times 10^{-9} \text{ F} \cdot \text{s}^{-1} \cdot \text{cm}^{-2}$ for CP3%, and $1 \times 10^{-9} \text{ F} \cdot \text{s}^{-1} \cdot \text{cm}^{-2}$ for CP5%.
- A transition of the leaching rate of calcium ions from the MSN-CP3% coating was observed after 2 days of immersion. The increased leaching rate after 2 days of exposure can be related to the decrease of the coating film resistance and the triggered released of the pigment inside the coating film.
- The higher leaching rate of inhibitive ions from the coating with the encapsulated inhibitive pigment (MSN-CP3%) leads to more efficient corrosion inhibition.
- Pigment encapsulation contributes to a more uniform coating microstructure, which provides good barrier properties of the coating film during exposure.

■ APPENDIX

Figure 10 shows the reproducibility check results of the electrochemical evaluation.

■ AUTHOR INFORMATION

Corresponding Author

Huichao Bi – CoaST, Department of Chemical and Biochemical Engineering, Technical University of Denmark (DTU), 2800 Kgs. Lyngby, Denmark; orcid.org/0000-0003-0418-0355; Email: hubi@kt.dtu.dk

Authors

Zoi Lamprakou – CoaST, Department of Chemical and Biochemical Engineering, Technical University of Denmark (DTU), 2800 Kgs. Lyngby, Denmark

Claus Erik Weinell – CoaST, Department of Chemical and Biochemical Engineering, Technical University of Denmark (DTU), 2800 Kgs. Lyngby, Denmark

Kim Dam-Johansen – CoaST, Department of Chemical and Biochemical Engineering, Technical University of Denmark (DTU), 2800 Kgs. Lyngby, Denmark

Complete contact information is available at:
<https://pubs.acs.org/10.1021/acsomega.2c07853>

Notes

The authors declare no competing financial interest.

■ ACKNOWLEDGMENTS

Financial support from the Hempel Foundation to CoaST (The Hempel Foundation Coatings Science & Technology Centre) is gratefully acknowledged.

■ REFERENCES

- (1) Funke, W.; Haagen, H. Empirical or Scientific Approach to Evaluate the Corrosion Protective Performance of Organic Coatings. *Ind. Eng. Chem. Prod. Res. Dev.* **1978**, *17*, 50–53.
- (2) Emad, S.; Morsch, S.; Hashimoto, T.; Liu, Y.; Gibbon, S. R.; Lyon, S. B.; Zhou, X. Leaching from coatings pigmented with strontium aluminium polyphosphate inhibitor pigment-evidence for a cluster-percolation model. *Prog. Org. Coatings* **2019**, *137*, No. 105340.
- (3) Grundmeier, G.; Schmidt, W.; Stratmann, M. Corrosion protection by organic coatings: Electrochemical mechanism and novel methods of investigation. *Electrochim. Acta* **2000**, *45*, 2515–2533.
- (4) Lyon, S. B.; Bingham, R.; Mills, D. J. Advances in corrosion protection by organic coatings: What we know and what we would like to know. *Prog. Org. Coatings* **2017**, *102*, 2–7.
- (5) Sørensen, P. A.; Kiil, S.; Dam-Johansen, K.; Weinell, C. E. Anticorrosive coatings: A review. *J. Coatings Technol. Res.* **2009**, *6*, 135–176.
- (6) Ma, I. A. W.; Ammar, S.; Kumar, S. S. A.; Ramesh, K.; Ramesh, S. A concise review on corrosion inhibitors: types, mechanisms and electrochemical evaluation studies. *J. Coat. Technol. Res.* **2022**, *19*, 241–268.
- (7) Rammelt, U.; Reinhard, G. Characterization of active pigments in damage of organic coatings on steel by means of electrochemical impedance spectroscopy. *Prog. Org. Coatings* **1994**, *24*, 309–322.
- (8) Hao, Y.; Liu, F.; Han, E. H.; Anjum, S.; Xu, G. The mechanism of inhibition by zinc phosphate in an epoxy coating. *Corros. Sci.* **2013**, *69*, 77–86.
- (9) Furman, S. A.; Scholes, F. H.; Hughes, A. E.; Lau, D. Chromate leaching from inhibited primers. Part II: Modelling of leaching. *Prog. Org. Coatings* **2006**, *56*, 33–38.
- (10) Ashrafi-shahri, S. M.; Ravari, F.; Seifzadeh, D. Smart organic/inorganic sol-gel nanocomposite containing functionalized mesoporous silica for corrosion protection. *Prog. Org. Coatings* **2019**, *133*, 44–54.

- (11) Habib, S.; Shakoob, R. A.; Kahraman, R. A focused review on smart carriers tailored for corrosion protection: Developments, applications, and challenges. *Prog. Org. Coatings* **2021**, *154*, No. 106218.
- (12) Ding, C.; Fu, J. Smart anticorrosion coatings based on nanocontainers. *Elsevier Inc.* **2020**, 413.
- (13) Wei, H.; Wang, Y.; Guo, J.; Shen, N. Z.; Jiang, D.; Zhang, X.; Yan, X.; Zhu, J.; Wang, Q.; Shao, L.; et al. Advanced micro/nanocapsules for self-healing smart anticorrosion coatings. *J. Mater. Chem. A* **2015**, *3*, 469–480.
- (14) Zahidah, K. A.; Kakoei, S.; Ismail, M. C.; Bothi Raja, P. Halloysite nanotubes as nanocontainer for smart coating application: A review. *Prog. Org. Coatings* **2017**, *111*, 175–185.
- (15) Hollamby, M. J.; Fix, D.; Dönch, L.; Borisova, D.; Möhwald, H.; Shchukin, D. Hybrid polyester coating incorporating functionalized mesoporous carriers for the holistic protection of steel surfaces. *Adv. Mater.* **2011**, *23*, 1361–1365.
- (16) Yeganeh, M.; Asadi, N.; Omid, M.; Mahdavian, M. An investigation on the corrosion behavior of the epoxy coating embedded with mesoporous silica nanocontainer loaded by sulfamethazine inhibitor. *Prog. Org. Coatings* **2019**, *128*, 75–81.
- (17) Shchukina, E.; Grigoriev, D.; Sviridova, T.; Shchukin, D. Comparative study of the effect of halloysite nanocontainers on autonomic corrosion protection of polyeoxy coatings on steel by salt-spray tests. *Prog. Org. Coatings* **2017**, *108*, 84–89.
- (18) Wonnie Ma, I. A.; Ammar, S.; Bashir, S.; Selvaraj, M.; Assiri, M. A.; Ramesh, K.; Ramesh, S. Preparation of Hybrid Chitosan/Silica Composites Via Ionotropic Gelation and Its Electrochemical Impedance Studies. *Prog. Org. Coatings* **2020**, *145*, No. 105679.
- (19) Zheludkevich, M. L.; Tedim, J.; Ferreira, M. G. S. 'Smart' coatings for active corrosion protection based on multi-functional micro and nanocontainers. *Electrochim. Acta* **2012**, *82*, 314–323.
- (20) Yeganeh, M.; Marashi, S. M.; Mohammadi, N. Smart Corrosion Inhibition of Mild Steel Using Mesoporous Silica Nanocontainers Loaded with Molybdate. *Int. J. Nanosci. Nanotechnol.* **2018**, *14* (2), 143–151.
- (21) Nazeer, A. A.; Madkour, M. Potential use of smart coatings for corrosion protection of metals and alloys: A review. *J. Mol. Liq.* **2018**, *253*, 11–22.
- (22) Falcón, J. M.; Otubo, J. M.; Aoki, I. V. Highly ordered mesoporous silica loaded with dodecylamine for smart anticorrosion coatings. *Surf. Coat. Technol.* **2016**, *303*, 319–329.
- (23) Sinko, J. Challenges of chromate inhibitor pigments replacement in organic coatings. *Prog. Org. Coatings* **2001**, *42*, 267–282.
- (24) de Lima-Neto, P.; de Araújo, A. P.; Araújo, W. S.; Correia, A. N. Study of the anticorrosive behaviour of epoxy binders containing non-toxic inorganic corrosion inhibitor pigments. *Prog. Org. Coatings* **2008**, *62*, 344–350.
- (25) Alibakhshi, E.; Ghasemi, E.; Mahdavian, M. Sodium zinc phosphate as a corrosion inhibitive pigment. *Prog. Org. Coatings* **2014**, *77*, 1155–1162.
- (26) Alibakhshi, E.; Ghasemi, E.; Mahdavian, M. Corrosion inhibition by lithium zinc phosphate pigment. *Corros. Sci.* **2013**, *77*, 222–229.
- (27) Alibakhshi, E.; Ghasemi, E.; Mahdavian, M. Optimization of potassium zinc phosphate anticorrosion pigment by taguchi experimental design. *Prog. Org. Coatings* **2013**, *76*, 224–230.
- (28) Alibakhshi, E.; Haddadi, S.A.; Motlagh, A. L.; Ghaderi, M.; Ramezanzadeh, B.; Mahdavian, M.; Arjmand, M.; Jalili, M. Epoxy nanocomposite coating based on calcium zinc phosphate with dual active/barrier corrosion mitigation properties. *Prog. Org. Coatings* **2022**, *163*, 106677.
- (29) Li, W.; Shi, L.; Zhang, J.; Cheng, J.; Wang, X. Double-layered surface decoration of flaky aluminum pigments with zinc aluminum phosphate and phytic acid–aluminum complexes for high-performance waterborne coatings. *Powder Technol.* **2020**, *362*, 462–473.
- (30) Kowalczyk, K.; Łuczka, K.; Grzmil, B. Preparation and characterization of anticorrosion polyurethane paints and coatings based on novel Zn-free phosphates. *J. Coatings Technol. Res.* **2015**, *12*, 153–165.
- (31) Heydarpour, M. R.; Zarrabi, A.; Attar, M. M.; Ramezanzadeh, B. Studying the corrosion protection properties of an epoxy coating containing different mixtures of strontium aluminum polyphosphate (SAPP) and zinc aluminum phosphate (ZPA) pigments. *Prog. Org. Coatings* **2014**, *77*, 160–167.
- (32) Vetere, V. F.; Romagnoli, R. Role of calcium acid phosphate as corrosion inhibitive pigment. *Br. Corros. J.* **1994**, *29*, 115–119.
- (33) Del Amo, B.; Romagnoli, R.; Vetere, V. F. Steel corrosion protection by means of alkyd paints pigmented with calcium acid phosphate. *Ind. Eng. Chem. Res.* **1999**, *38*, 2310–2314.
- (34) Zin, I. M.; Pokhmurskii, V. I.; Scantlebury, J. D.; Lyon, S. B. Model Electrochemical Cell Study of Cut-Edge Corrosion Inhibition on Coil-Coated Steel Sheet by Chromate-, Phosphate-, and Calcium-Containing Pigments. *J. Electrochem. Soc.* **2001**, *148*, B293.
- (35) Łuczka, K.; Grzmil, B.; Michalkiewicz, B.; Kowalczyk, K. Studies on obtaining of aluminium phosphates modified with ammonium, calcium and molybdenum. *J. Ind. Eng. Chem.* **2015**, *23*, 257–264.
- (36) Borisova, D.; Mohwald, H.; Shchukin, D. G. Mesoporous silica nanoparticles for active corrosion protection. *ACS Nano* **2011**, *5*, 1939–1946.
- (37) Li, W.; Liu, A.; Tian, H.; Wang, D. Controlled release of nitrate and molybdate intercalated in Zn-Al-layered double hydroxide nanocontainers towards marine anticorrosion applications. *Colloids Interface Sci. Commun.* **2018**, *24*, 18–23.
- (38) Lamprakou, Z.; Bi, H.; Weinell, C. E.; Tortajada, S.; Dam-Johansen, K. Smart epoxy coating with mesoporous silica nanoparticles loaded with calcium phosphate for corrosion protection. *Prog. Org. Coatings* **2022**, *165*, No. 106740.
- (39) Prosek, T.; Thierry, D. A model for the release of chromate from organic coatings. *Prog. Org. Coatings* **2004**, *49*, 209–217.
- (40) Emad, S.; Zhou, X.; Lyon, S. B.; Thompson, G. E.; Liu, Y.; Smyth, G.; Graham, D.; Francis, D.; Gibbon, S. R. Influence of volume concentration of active inhibitor on microstructure and leaching behaviour of a model primer. *Prog. Org. Coatings* **2017**, *102*, 71–81.
- (41) Emad, S.; Zhou, X.; Morsch, S.; Lyon, S. B.; Liu, Y.; Graham, D.; Gibbon, S. R. How pigment volume concentration (PVC) and particle connectivity affect leaching of corrosion inhibitive species from coatings. *Prog. Org. Coatings* **2019**, *134*, 360–372.
- (42) Lamprakou, Z.; Bi, H.; Weinell, C. E.; Dam-Johansen, K. Tannin-based inhibitive pigment for sustainable epoxy coatings formulation. *Prog. Org. Coatings* **2022**, *167*, No. 106841.
- (43) Wonnie Ma, I. A.; Kumar, S. S. A.; Kasi, R.; Shafaamri, A.; Subramaniam, R. A comparative study of corrosion resistance of epoxy-based coating incorporated chitosan, silica and hybrid compound of chitosan/silica on mild steel. *Pigment & Resin Technology*, **2022**, DOI: 10.1108/PRT-08-2021-0094.
- (44) McIntyre, J. M.; Pham, H. Q. Electrochemical impedance spectroscopy; a tool for organic coatings optimizations. *Prog. Org. Coatings* **1996**, *27*, 201–207.
- (45) Deflorian, F.; Fedrizzi, L.; Rossi, S.; Bonora, P.L. Organic coating capacitance measurement by EIS: ideal and actual trends. *Electrochim. Acta* **1999**, *44*, 4243–4249.
- (46) Wonnie Ma, I.A.; Ammar, S.; Shahid, B.; Kumar, S. S. A.; Ramesh, K.; Ramesh, S. Development of active barrier effect of hybrid chitosan/silica composite epoxy-based coating on mild steel surface. *Surfaces and Interfaces* **2011**, *25*, No. 101250.